Received February 15, 2020, accepted February 27, 2020, date of publication March 3, 2020, date of current version March 13, 2020.

Digital Object Identifier 10.1109/ACCESS.2020.2978092

Multi-Objective Optimization Dispatching Strategy for Wind-Thermal-Storage Generation System Incorporating Temporal and Spatial Distribution Control of Air Pollutant Dispersion

ZHUOHUAN LI, TAO YU, (Member, IEEE), YIXUAN CHEN, HANXIN ZHU, AND WEICONG WU
School of Electric Power Engineering, South China University of Technology, Guangzhou 510640, China

Corresponding author: Tao Yu (taoyu1@scut.edu.cn)

This work was supported in part by the National Natural Science Foundation of China under Grant 51777078.

ABSTRACT Temporal and spatial distribution (TSD) model presented in our previous work of air pollutants is an effective model in describing the increment ground level concentration caused by power generation. In this paper, the newly emerging temporal and spatial characteristics of power dispatch when incorporating the TSD model are studied. Firstly, a multi-objective optimization dispatching model for wind-thermal-storage generation system is proposed. In the time dimension, the model can coordinate multiple generation sources in the face of atmospheric condition variation. In the space dimension, the correlations between power plants location, pollutant diffusion paths and atmospheric boundary layers are considered. Secondly, chance constraints are adopted to address stochastic variables, while the stochastic formulation is transformed into a deterministic one based on wind power distribution. Then a multi-objective optimization method is employed to obtain a desired Pareto front. Case studies are carried out on modified IEEE 39-bus system and Guangdong grid system under four strategies, which validate the performance of the proposed model and the effectiveness of the strategy.

INDEX TERMS Environmental economic dispatch, comprehensive pollution evaluation value, geographic grid, temporal and spatial characteristics, multi-objective optimization.

NOMENCLATURE

INDICES

i	Index of thermal power unit, $i = 1, \ldots, N$
j	Index of air quality monitoring points, $j = 1, \ldots, N_j$
t	Index of scheduling time interval, $t = 1, \ldots, T$
τ	Index of puff emitted time interval
t'	Index of monitoring time

PARAMETERS

T_{res}	Termed residence period
Δt	Time interval between the two monitoring times
$x_s/y_s/z_s$	Geographic coordinate of the thermal power units in dimension $x/y/z$
$x_c/y_c/z_c$	Geographic coordinate of the center of the emitted puff in dimension $x/y/z$
x_j/y_j	Geographic coordinate of the monitoring station j in dimension x/y
$u/v/w$	Average wind speed in dimension $x/y/z$
$\sigma_x/\sigma_y/\sigma_z$	Parameters of dispersion in dimension $x/y/z$
$\alpha/\beta/\lambda/\gamma$	Calculation coefficients of dispersion parameters
z_i	Height of the ABL at unit i
$v_{in}/v_r/v_{out}$	Cut-in/rated/cut-out wind speed of the wind turbine
P_r	Rated output of the wind farm.
$a_i/b_i/c_i$	Power generation cost coefficients of unit i
$d_i/e_i/g_i$	CO_2 emission coefficients of unit i
$h_i/l_i/m_i$	SO_2 emission coefficients of unit i
P_{Wt}	Wind power generation output at time t
P_{Dt}	System load demand at time t

The associate editor coordinating the review of this manuscript and approving it for publication was Lin Zhang.

D_{Ri} /U_{Ri}	Downward/upward ramping rate of unit i
$P_{it}^{\max}/P_{it}^{\min}$	Upper/lower limit of generation output of thermal power unit i
$P_W^{\max}$	Upper limit of wind power generation output
U_{SRt}	Reserve capacity demand at time t
w_u/w_d	Positive/ negative reserve demand coefficient of wind power generation output
$P^g_{Ht,\min}/P^g_{Ht,\max}$	Lower/upper power generation limit of the pumped storage plant
$P^p_{Ht,\min}/P^p_{Ht,\max}$	Lower/upper pumping power limit of the pumped storage power plant
$E_{Ht,\min}/E_{Ht,\max}$	Lower/upper limit of water storage capacity
$\eta^{\mathrm{g}}/\eta^{\mathrm{p}}$	Power generation/ pumping efficiency of the pumped storage power plant

VARIABLES

P_{it}	Power output of unit i at time t
P^g_{Ht}/P^p_{Ht}	Output of the pumped storage power unit at time t working in generation/pumping state
μ^g_t/μ^p_t	Binary generation/pumping decision of the pumped storage power unit at time t
E_{Ht}	Water storage capacity of pumped storage power plant at time t

ABBREVIATIONS

EED	Environmental economic dispatch
GLPC	Ground level pollutant concentration
ABL	Atmospheric boundary layer
TSD	Temporal and spatial distribution
EL	Entrainment layer
ML	Mixed layer
SBL	Stable boundary layer
RL	Remaining layer
CPEV	Comprehensive pollution evaluation value
NBI	Normal boundary intersection

I. INTRODUCTION

Air pollution has been one of the most serious environmental risks in the world [1]. In China, 31% of SO_2 emissions and 30% of NO_x emissions are contributed by electricity generation [2]. In the USA, 75% SO_2 emissions are contributed by power plants in 1980s while still 1.26 million tons in 2018, causing severe acid rain.

In this context, environmental economic dispatch (EED) has been a hot topic due to its low-cost merits. Reduction of air pollutants emissions has been widely considered in the existing research [3]–[5] by imposing penalty cost, introducing constraints [6]–[8], or developing a multi-objective EED model which takes emission as a separate objective [9], [10]. However, it should be noted that ground level pollutant concentration (GLPC) is actually the essential aim of environmental production, which directly determines the level of health hazards and economic losses [11], [12]. GLPC is not only related to pollutants emissions, but also influenced by the characteristics of the pollutant source and the dispersion process.

To conduct EED from the perspective of controlling GLPC, the complex chemical and physical mechanism of pollutant diffusion and the resulting GLPC needs to be studied. A plume model is employed in [12] to describe the dispersion process. In environment science, Gaussian plume model is widely applied in the case where pollutant source release pollutants continuously and the pollutants disperse in limited range. However, Gaussian plume model is not suitable in the situations where the wind is light or calm. Moreover, the diurnal variation of wind conditions and atmospheric conditions are ignored. By contrast, Gaussian puff model is adopted by [13] and [14] to simulate air pollutants movement and dispersion, but the influence of diurnal variation of atmospheric boundary layer (ABL) on air pollutants dispersion is not considered.

In our preliminary work, we developed a temporal and spatial distribution (TSD) model of air pollutants [15]. The TSD model can well describe the significant correlations between GLPC and the ABL's diurnal variation. This model was proved effective in reducing GLPC when employed in power dispatch. However, the newly emerging temporal and spatial characteristics of power dispatch when incorporating TSD model are still not clear, while the impacts of renewable energy penetration also requires further research.

Wind power generation plays an important role in reducing pollutants emissions [16]–[21]. However, wind power output is intermittent, and its positive effects in environmental protection cannot be seen in light and calm wind conditions. Pumped storage power plants play an active role in peak cut by generating power at the peaks of system load and pumping at the valleys. Similarly, as a typical energy storage way in power system, if they are applied to EED by generating power when GLPC is high and pumping when GPLC is low, then peak cut in GPLC can be achieved. Therefore, it is necessary to grasp the temporal characteristics of the distribution of pollutants and coordinate with the scheduling of the pumped storage plants.

Based on the TSD model described in our previous work, we focus on studying the temporal and spatial characteristics of the TSD model. The main contributions of this paper are as follows.

1) A multi-objective optimization dispatching model for wind-thermal-storage generation system considering temporal and spatial distribution control of air pollutants is proposed. In the time dimension, the model can coordinate multiple generation sources in the face of atmospheric condition variation. In the space dimension, the correlations between power plants location, pollutant diffusion paths and atmospheric boundary layers are considered.

2) Geographic grid point interpolation method is adopted to evaluate the wind speed at each geographic location and along the puff center moving path.

3) Chance constraints are employed to process random variables in the model. Then based on the distribution function of wind power generation output, we transform the uncertain problem into a deterministic one, while multi-objective optimization method is employed to handle the problem.

4) Several strategies to make EED plan are developed and discussed. A modified IEEE 39-bus system and Guangdong Grid system are employed to demonstrate the validity and feasibility of the proposed model, while the simulation in this paper is carried out under two different meteorological conditions.

This paper is organized as follows. In section II, TSD model of air pollutants is introduced while section III presents the multi-objective optimization dispatching model for wind-thermal-storage generation system considering TSD model. In section IV, the method and the process to handle the dispatching problem is described. Case studies are included in Section V for illustration. Section VI concludes this paper.

II. TSD MODEL OF AIR POLLUTANTS

A. BASIC FRAME

Gaussian puff model simulates the dispersion of pollutants by decomposing the continuous plume into dispersed puff [22]. The GLPC at a monitoring station (x, y, z) and at monitoring time t' caused by a thermal power unit i is calculated by summing the effects of all puffs which are emitted during $[t'\text{-}T_{res}, t'\text{-}1]$, where T_{res} is the average life span of air pollutants in the atmosphere (termed residence period), representing the physical-chemical attenuation of pollutants. Therefore, *GLPC* can be formulated as

$$GLPC(t'; x, y, z) = \sum_{i=1}^{N} \sum_{\tau=t'-T_{res}}^{t'-1} Q_i(\tau) G_i(\tau, t'; x, y, z) \times \exp\left(-\frac{t'-\tau}{T_{res}}\right) \quad (1)$$

where N is the number of thermal power units; τ and t' are the time of pollutants emission and the monitoring time; x, y, and z are the three-dimensional geographic coordinates of the monitoring station, where $z = 0$ is often set; $Q_i(\tau)$ is the mass of the puff emitted by the unit i at time τ. $G_i(\cdot)$ is the dispersion distribution function, which can be formulated as follows without considering the effects of ABL.

$$\begin{aligned} &G_i(\tau, t'; x, y, z) \\ &= \left[(2\pi)^{3/2}\sigma_x(\tau, t')\sigma_y(\tau, t')\sigma_z(\tau, t')\right]^{-1} \\ &\quad \times \exp\left\{-\frac{1}{2}\left[\left(\frac{x - x_c(\tau, t')}{\sigma_x(\tau, t')}\right)^2 + \left(\frac{y - y_c(\tau, t')}{\sigma_y(\tau, t')}\right)^2 \right.\right. \\ &\quad \left.\left. + \left(\frac{z - z_c(\tau, t')}{\sigma_z(\tau, t')}\right)^2\right]\right\} \end{aligned} \quad (2)$$

where $\sigma_x(\tau, t')$, $\sigma_y(\tau, t')$, $\sigma_z(\tau, t')$ are the parameters of dispersion in three dimension x, y and z.

$x_c(\tau, t')$, $y_c(\tau, t')$, $z_c(\tau, t')$ is the coordinate of the center of the emitted puff, which is constantly updated at different monitoring times, as

$$\begin{bmatrix} x_c(\tau, t') \\ y_c(\tau, t') \\ z_c(\tau, t') \end{bmatrix} = \begin{bmatrix} x_s \\ y_s \\ z_s \end{bmatrix} + \sum_{t=\tau+1}^{t'} \begin{bmatrix} u(t) \\ v(t) \\ w(t) \end{bmatrix} \Delta t \quad (3)$$

where x_s, y_s, z_s are the three-dimensional geographic coordinates of the pollution source of the thermal power units; t is index of time intervals; Δt is the time interval between the two monitoring times, and $\Delta t = 1$ h in this paper; $u(t)$, $v(t)$, $w(t)$ are the average wind speeds in the three directions x, y and z within the time interval Δt.

If the atmospheric conditions remain stable within the time interval $[\tau, t]$, dispersion parameters satisfy

$$\begin{cases} \sigma_x(\tau, t) = \sigma_y(\tau, t) = \alpha(t)(t - \tau)^{\lambda(t)} \\ \sigma_z(\tau, t) = \beta(t)(t - \tau)^{\gamma(t)} \end{cases} \quad (4)$$

where α, β, λ, γ are the calculation coefficients of the dispersion parameters, which depend on the atmospheric stability level of the puff center at each moment.

If the atmospheric stability level changes at the time $t+\Delta t$, the atmospheric dispersion parameters follow the continuous transition relationship, as

$$\begin{cases} \sigma_y(\tau, t) = \alpha(t)(t - \tau)^{\lambda(t)} \\ \quad = \alpha(t + \Delta t)(t - \tau + \Delta\delta_y)^{\lambda(t+\Delta t)} \\ \sigma_z(\tau, t) = \beta(t)(t - \tau)^{\gamma(t)} \\ \quad = \beta(t + \Delta t)(t - \tau + \Delta\delta_z)^{\gamma(t+\Delta t)} \end{cases} \quad (5)$$

where $\Delta\delta_y$ and $\Delta\delta_z$ are translation variables introduced to ensure continuous transition of dispersion parameters.

The following two equations are obtained by solving Equation (5):

$$\begin{cases} \Delta\delta_y = \left[\alpha(t + \Delta t)^{-1}\sigma_y(\tau, t)\right]^{1/\lambda(t+\Delta t)} - (t - \tau) \\ \Delta\delta_z = \left[\alpha(t + \Delta t)^{-1}\sigma_z(\tau, t)\right]^{1/\gamma(t+\Delta t)} - (t - \tau) \end{cases} \quad (6)$$

$$\begin{cases} \sigma_y(\tau, t + \Delta t) \\ \quad = \left[\alpha(t + \Delta t)^{1/\lambda(t+\Delta t)}\Delta t + \sigma_y(\tau, t)^{1/\lambda(t+\Delta t)}\right]^{\lambda(t+\Delta t)} \\ \sigma_z(\tau, t + \Delta t) \\ \quad = \left[\beta(t + \Delta t)^{1/\gamma(t+\Delta t)}\Delta t + \sigma_z(\tau, t)^{1/\gamma(t+\Delta t)}\right]^{\gamma(t+\Delta t)} \end{cases} \quad (7)$$

B. TSD OF AIR POLLUTANTS CONSIDERING THE INFLUENCE OF ABL

The atmospheric boundary layer shows obvious diurnal variation with solar radiation and temperature variation. The diurnal variation of its structure is shown in Figure 1 [23]. Correspondingly, pollutants dispersion presents three different types, namely fumigation, enclosed type and downward inhibited type.

During the daytime, ABL consists of an unstable mixed layer (ML) and a stable entrainment layer (EL). The height of the daytime ABL, i.e., z_i, refers to the bottom of the

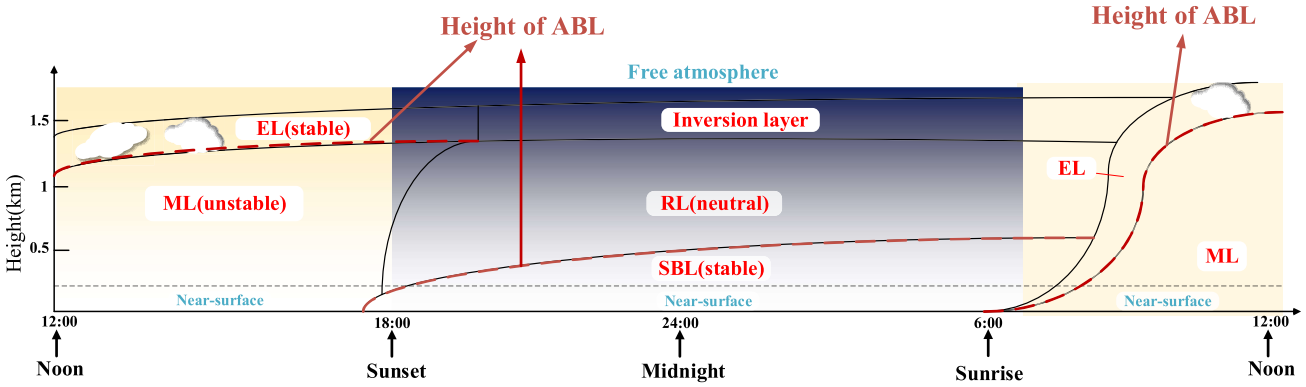

FIGURE 1. Diurnal variation of atmospheric boundary layer.

unstable ML. If z_i has not exceeded z_s, the pollutants disperse following fumigation, or enclosed type.

After sunset, the stable boundary layer (SBL) begins to form from the ground, while the daytime ML gradually becomes a neutral remaining layer (RL), which exists above the SBL. The ABL height z_i, is the height at of the top of SBL and pollutants disperse following downward inhibited type.

FUMIGATION

In the early morning when z_i is normally lower than z_s, the pollutants will be directly emitted and accumulated in the upper SBL. As the ABL height continually rises, the upward movements of the originally stable pollutants is suppressed by the upper stable EL, while are dominated by the lower active thermal turbulent exchange. Therefore, they disperse and mix up down vertically to the ground, increasing the ground concentration significantly. This process continues to develop and reaches the climax as the inversion layer subsides to the upper edge of the plume. Thereafter, the pollutants are completely emitted into the unstable ML, the peak concentration decreases, and the fumigation process ends. Fumigation can be formulated as

$$\begin{cases} G_i(\tau,t';x,y) = \dfrac{\int_{-\infty}^{p}\exp\left(-p^2/2\right)\mathrm{d}p}{(2\pi)^{\frac{3}{2}}\sigma_{y\mathrm{F}}^2(\tau,t')z_i(t)} \\ \times\exp\left(-\dfrac{\left[x-x_c(\tau,t')\right]^2+\left[y-y_c(\tau,t')\right]^2}{2\sigma_{y\mathrm{F}}^2(\tau,t')}\right), \\ \quad \text{if } \left[S(\tau)\geq 4|z_{si}>z_i(\tau)\right]\&S(t)<4 \\ \sigma_{y\mathrm{F}}(\tau,t') = \sigma_{ys}(\tau,t')+z_c(\tau,t')/8 \\ p(t') = \left[z_i(t)-z_c(\tau,t')\right]/\sigma_{zs}(\tau,t') \end{cases} \tag{8}$$

where $S(t)$ is the atmospheric stability level below the height of the ABL at time t. According to GB/T 3840-91 [24], the atmospheric stability level is divided into 9 levels. The smaller the stability level is, the more unstable the atmosphere is. $S(t)$ =4 indicates that the atmospheric stability is neutral; $[S(\tau)\geq 4|z_{si}>z_i(\tau)]$ indicates that the pollutants are initially emitted into a stable layer; $S(t)$ <4 indicates that the ML is formed and the height of the ML increases; σ_{ys} and σ_{zs} is the horizontal and vertical dispersion coefficient when the pollutants staying in the SBL; σ_{yF} is the horizontal dispersion coefficient after the pollutants enter the unstable ML.

ENCLOSED TYPE

From noon to sunset, the pollutants are emitted into the ML, which is under the EL. The EL is an inversion layer whose properties are very stable and where the turbulent exchange is weak, suppressing the vertical dispersion of pollutants. Therefore, the pollutants are enclosed between the EL and the earth and are reflected by multiple times, which can be formulated as

$$\begin{cases} G_i(\tau,t';x,y) = \dfrac{\exp\left[-\dfrac{1}{2}\left(\dfrac{y-y_c(\tau,t')}{\sigma_y(\tau,t')}\right)^2\right]R(\tau,t')}{(2\pi)^{3/2}\sigma_y^2(\tau,t')\sigma_z(\tau,t')} \\ \text{, if} S(\tau)<4\&z_{si}\leq z_i(\tau)\&S(t)<4 \\ R(\tau,t') = \sum\limits_{n=-N_R}^{N_R}\exp\left[-\dfrac{\left(2nz_i(t)-z_c(\tau,t')\right)^2}{2\sigma_z^2(\tau,t')}\right] \\ +\sum\limits_{n=-N_R}^{N_R}\exp\left[-\dfrac{\left(2nz_i(t)+z_c(\tau,t')\right)^2}{2\sigma_z^2(\tau,t')}\right] \end{cases} \tag{9}$$

where $S(\tau)$ <4&$z_{si}\leq z_i(\tau)$&$S(t)$ <4 indicates that the puff is emitted into the unstable ML; N_R is the number of reflections of the pollutants puff, N_R =4 is set in this paper.

DOWNWARD INHIBITED TYPE

After sunset, the radiation on the ground is weakened and the SBL begins to form from the ground. The most commonly used method for estimating the dispersion in SBL is the P-G stability dispersion method. In this paper, the method is used to modify the value of α, β, λ and γ according to the stability level of the atmosphere where the pollutants puff stays, and then the puff dispersion coefficient is modified according to (5). In this period, the condition of atmospheric stability level is $S(t)$ >4, and the pollutants is emitted into the SBL or the RL. In this scenario, the dispersion process can be formulated as

$$G_i(\tau,t';x,y) = \left[(2\pi)^{3/2}\sigma_{yw}^2(\tau,t')\sigma_{zw}(\tau,t')\right]^{-1}$$

$$\times \exp\left\{-\frac{1}{2}\left[\left(\frac{x-x_c(\tau,t')}{\sigma_{xw}(\tau,t')}\right)^2+\left(\frac{y-y_c(\tau,t')}{\sigma_{yw}(\tau,t')}\right)^2 +\left(\frac{z-z_c(\tau,t')}{\sigma_{zw}(\tau,t')}\right)^2\right]\right\} \tag{10}$$

where σ_{xw}, σ_{yw}, σ_{zw} are modified dispersion coefficient.

III. MULTI-OBJECTIVE OPTIMIZATION DISPATCHING MODEL FOR WIND-THERMAL-STORAGE GENERATION SYSTEM CONSIDERING TSD MODEL

A. WIND SPEED INTERPOLATION METHOD BASED ON GEOGRAPHIC GRID

In order to evaluate the wind speed at each geographic location and along the puff center moving path, grid point interpolation method is adopted as follows.

$$f(x,y)=\sum_{j=1}^{N_j} f_j * W(r_j)/\sum_{j=1}^{N_j} W(r_j) \tag{11}$$

where f_j is observation data at wind speed observation station j; r_j is the geographical distance from the grid point (x, y) to observation station (x_j, y_j), which satisfies

$$r_j=\sqrt{(x-x_j)^2+(y-y_j)^2} \tag{12}$$

$W(r)$ is a weight interpolation function as

$$W(r)=\begin{cases}\dfrac{R^2-r^2}{R^2+r^2} & r\le R\\ 0 & r>R\end{cases} \tag{13}$$

where R is the influence radius, which indicates that the station beyond the distance R has no effect on the value of the grid point. In (3), $u(t)$, $v(t)$ and $w(t)$ are all obtained by interpolation method.

B. PROBABILISTIC MODEL OF WIND POWER GENERATION OUTPUT

This paper simulates the distribution of wind speed with a normal distribution based on predicted wind speed, as

$$\hat{v}_t \sim N(\bar{v}_t, \sigma_t^2) \tag{14}$$

where $\bar{v}_t$ is the average wind speed value using the geographic grid interpolation method at the wind farm location at time t; σ_t is the standard deviation of the wind speed at time t.

The function relationship between wind farm output P_{Wt}, and wind speed $\hat{v}_t$ can be formulated as

$$P_{Wt}=\begin{cases}0, & \hat{v}_t<v_{in}\ or\ \hat{v}_t\ge v_{out}\\ P_r\dfrac{\hat{v}_t-v_{in}}{v_r-v_{in}}, & v_{in}\le\hat{v}_t<v_r\\ P_r, & v_r\le\hat{v}_t<v_{out}\end{cases} \tag{15}$$

where v_{in}, v_r and v_{out} are the cut-in wind speed, rated wind speed, and cut-out wind speed of the wind turbine respectively; P_r is the rated output of the wind farm.

Then, the distribution function of wind power generation output can be obtained, as

$$F(P_{Wt})=\begin{cases}0, & P_{Wt}<0\\ N\left(\dfrac{P_r}{v_r-v_{in}}\bar{v}_t-\dfrac{P_r\cdot v_{in}}{v_r-v_{in}},\ \dfrac{P_r}{v_r-v_{in}}\cdot\sigma_t\right), & 0\le P_{Wt}\le P_r\\ 1, & P_{Wt}>P_r\end{cases} \tag{16}$$

C. OBJECTIVE FUNCTION

1) OBJECTIVE 1: POWER GENERATION COST

The system power generation cost F_C can be formulated as

$$F_C=\sum_{t=1}^{T}\sum_{i=1}^{N}F_{Ci}(P_{it}) \tag{17}$$

$$F_{Ci}(P_{it})=a_i+b_iP_{it}+c_iP_{it}^2 \tag{18}$$

where T is the number of hours in the dispatching horizon, and $T = 24$ is set in this paper; N is the number of thermal power units; P_{it} is the power output of unit i at time t; $F_{Ci}(P_{it})$ is the consumption function of unit i; a_i, b_i and c_i are the power generation cost coefficients of unit i.

2) OBJECTIVE 2: CARBON EMISSIONS

$$E_C=\sum_{t=1}^{T}\sum_{i=1}^{N}E_{Ci}(P_{it}) \tag{19}$$

$$E_{Ci}(P_{it})=d_i+e_iP_{it}+g_iP_{it}^2 \tag{20}$$

where $E_{Ci}(P_{it})$ is the carbon emission function of unit i; d_i, e_i and g_i are the CO_2 emission coefficients of unit i.

3) OBJECTIVE 3: AVERAGE COMPREHENSIVE POLLUTION EVALUATION VALUE

The purpose of this paper is to reduce the GLPC caused by thermal power units. Therefore, it is necessary to comprehensively consider the meteorological conditions on the scheduling day and the spatial and temporal distribution characteristics of atmospheric pollution to comprehensively evaluate the impact of pollutants.

The GLPC impacts of pollutants on air quality sustains during the following T_{res}. Therefore, the cumulative GLPC in $[\tau, \tau + T_{res}]$ for all the pollutants emitted by thermal power units at τ are taken as the comprehensive pollution evaluation value (CPEV) and the average CPEV of all pollutants emitted in the scheduling day is the third objective as

$$\overline{CPEV}=\sum_{\tau=1}^{T}\sum_{t'=\tau}^{\tau+T_{res}}\sum_{i=1}^{N}\sum_{j=1}^{N_j}Q_i(\tau)G_i(\tau,t';x_j,y_j) \times\exp\left(-\frac{t'-\tau}{T_{res}}\right)/N_j \tag{21}$$

$$Q_i(\tau)=h_i+l_iP_{it}+m_iP_{it}^2 \tag{22}$$

where N_j is the number of air quality monitoring points; (x_j, y_j) is the geographic coordinates of the monitoring station j; $Q_i(\tau)$ is the mass of puff emitted by unit i at time τ; h_i, l_i and m_i are SO_2 emission coefficients of unit i.

D. CONSTRAINTS

1) SUPPLY AND DEMAND BALANCE CONSTRAINTS

The supply and demand balance constraints of the system are given by:

$$\sum_{i=1}^{N} P_{it} + P_{Wt} + \mu_t^g P_{Ht}^g - \mu_t^p P_{Ht}^p = P_{Dt} \tag{23}$$

where P_{Wt} is the wind power generation output at time t; μ_t^g, μ_t^p are 0-1 variables representing pumped storage power units working in generation/pumping states, while P_{Ht}^g, P_{Ht}^p are the corresponding outputs; P_{Dt} is the system load demand at time t.

2) RAMPING RATE CONSTRAINTS

The ramping rate constraints of thermal units are given by:

$$D_{Ri} \le P_{it} - P_{i(t-1)} \le U_{Ri} \tag{24}$$

where D_{Ri} /U_{Ri} is downward/upward ramping rate of unit i.

3) SPINNING RESERVE CAPACITY CONSTRAINTS

In order to handle the randomness of wind power generation output, chance constraint method is employed to handle the spinning reserve capacity constraints:

$$\begin{cases} P(\sum_{i=1}^{N} (P_i^{\max} - P_{it}) + R_{Ht}^g \ge U_{SRt} + w_u P_{Wt}) \ge \beta_1 \\ P(\sum_{i=1}^{N} (P_{it} - P_i^{\min}) + R_{Ht}^p \ge w_d (P_W^{\max} - P_{Wt})) \ge \beta_2 \end{cases} \tag{25}$$

where $P_{it}^{\max}/P_{it}^{\min}$ is upper/lower limit of generation output of thermal power unit i, $P_W^{\max}$ is upper limit of wind power generation output;U_{SRt} is the reserve capacity demand at time t; w_u/w_d is the positive/ negative reserve demand coefficient of wind power generation output; β_1 and β_2 are confidence coefficients. In this paper, β_1, β_2 =0.95.

4) GENERATION OUTPUT LIMIT CONSTRAINTS OF CONVENTIONAL UNITS

The output limit constraints of conventional units are given by:

$$P_{it}^{\min} \le P_{it} \le P_{it}^{\max} \tag{26}$$

5) OPERATIONAL CONSTRAINTS OF THE PUMPED STORAGE POWER PLANT

The operational constraints of the pumped storage power plant are given by:

$$P_{Ht,\min}^g \le P_{Ht}^g \le P_{Ht,\max}^g \tag{27}$$

$$P_{Ht,\min}^p \le P_{Ht}^p \le P_{Ht,\max}^p \tag{28}$$

$$E_{H,\min} \le E_{Ht} \le E_{H,\max} \tag{29}$$

$$\mu_t^g + \mu_t^p \le 1 \tag{30}$$

$$E_{Ht} = E_{H,t-1} + \Delta t(\mu_t^p P_{Ht}^p \eta^p - \mu_t^g P_{Ht}^g / \eta^g) \tag{31}$$

where $P_{Ht,\min}^g/P_{Ht,\max}^g$ is the lower/upper power generation limit of the pumped storage plant;$P_{Ht,\min}^p/P_{Ht,\max}^p$ is the lower/upper pumping power limit of the pumped storage power plant; E_{Ht} is water storage capacity of pumped storage power plant and $E_{Ht,\min}/E_{Ht,\max}$ is its lower/upper limit; η^g, η^p are power generation and pumping efficiency of the pumped storage power plant.

In order to facilitate periodic scheduling and ensure the long-term operation of the system, the daily remaining capacity of pumped storage is set to be greater than the daily initial capacity, as follows:

$$E_{H,1} \le E_{H,24} \tag{32}$$

IV. SOLUTION ALGORITHM

A. CHANCE CONSTRAINTS TRANSFORMATION

According to the distribution function of wind power generation output, Equation (25) can be transformed into [25], [26]

$$\begin{cases} P\left(P_{Wt} \le \dfrac{1}{w_u}\left[\sum_{i=1}^{N}(P_{it}^{\max} - P_{it}) + R_{Ht}^g - U_{SRt}\right]\right) \ge \beta_1 \\ P\left(P_{Wt} \ge P_r - \dfrac{1}{w_d}\sum_{i=1}^{N}\left(P_{it} - P_{it}^{\min}\right) - \dfrac{1}{w_d}R_{Ht}^p\right) \ge \beta_2 \end{cases} \tag{33}$$

Then, we obtain

$$\begin{cases} \dfrac{1}{w_u}\left[\sum_{i=1}^{N}(P_{it}^{\max} - P_{it}) + R_{Ht}^g - U_{SRt}\right] \ge \Phi^{-1}(\hat{P}_{Wt}, \sigma_W, \beta_1) \\ P_r - \dfrac{1}{w_d}\sum_{i=1}^{N}\left(P_{it} - P_{it}^{\min}\right) - \dfrac{1}{w_d}R_{Ht}^p \le \Phi^{-1}(\hat{P}_{Wt}, \sigma_W, 1-\beta_2) \end{cases} \tag{34}$$

where Φ^{-1} is the inverse function of the normal distribution function; $\hat{P}_{Wt}$ is the predicted value of wind power generation output at time t; σ_w is the standard deviation of wind power generation output and $\sigma_W = P_W^{\max}/(v_r - v_{in})$.

B. MULTI-OBJECTIVE OPTIMIZATION METHOD

After transforming the chance constraints in the spinning reserve capacity constraints, the normal boundary intersection (NBI) method is employed to solve the three-objective optimization problem in this paper. NBI is proposed by Indraneel Das and J. E. Dennis [27], and is proved independent of the relative scales of the functions and is successful in producing an evenly distributed set of points in the Pareto set given an evenly distributed set of parameters. Further, this method can handle more than two objectives while retaining the computational efficiency of continuation-type algorithms. In [28], it is proved that NBI produces better representation of Pareto front in power system analysis. By employing NBI, a set of uniformly distributed Pareto optimal solutions are obtained [29]–[31]. Detailed solution steps are as follows:

1) OBJECTIVE FUNCTION NORMALIZATION

$$\bar{f}_i = \frac{f_i - \hat{f}_i}{\check{f}_i - \hat{f}_i} \qquad i = 1, 2, 3 \tag{35}$$

where f_i is the objective function value, in this paper, it is generation cost, carbon emissions and the comprehensive pollution evaluation value; $\hat{f}_i, \check{f}_i$ are positive and negative idea point, as

$$\begin{aligned} \hat{f}_i &= f_i(x^{i*}) \\ \check{f}_i &= \max\left\{f_i(x^{1*}), f_i(x^{2*}), f_i(x^{3*})\right\} \quad i = 1, 2, 3 \end{aligned} \tag{36}$$

where, x^{i*} is the optimal solution obtained when single-objective optimization is performed with the objective i.

2) UNIFORMLY DISTRIBUTED POINTS GENERATION

The points on the utopian surface can be represented by a linear combination of the endpoints f^{i*} of the utopian surface, as

$$f^{i*} = (f_1(x^{i*}), f_2(x^{i*}), f_3(x^{i*})) \qquad i = 1, 2, 3 \tag{37}$$

The jth uniformly distributed point on the utopia surface can be expressed as

$$p_j = A\alpha = \begin{bmatrix} \bar{f}_1(x^{1*}) & \bar{f}_1(x^{2*}) & \bar{f}_1(x^{3*}) \\ \bar{f}_2(x^{1*}) & \bar{f}_2(x^{2*}) & \bar{f}_2(x^{3*}) \\ \bar{f}_3(x^{1*}) & \bar{f}_3(x^{2*}) & \bar{f}_3(x^{3*}) \end{bmatrix} \begin{bmatrix} \alpha_{1j} \\ \alpha_{2j} \\ \alpha_{3j} \end{bmatrix} \tag{38}$$

where $\alpha_{ij} = [1/H, 2/H, \ldots, H/H]$ and $\sum \alpha_{ij} = 1$; H is the number of interval segments.

3) PARETO OPTIMAL SOLUTION

The mathematical model for calculating the intersections of the axis vector, i.e., $\boldsymbol{n}$, and the Pareto front is as follows:

$$\begin{aligned} &\min(-d) \\ &s.t. \begin{cases} p_{1j} = r_{1j} + d \cdot n_1 \\ p_{2j} = r_{2j} + d \cdot n_2 \\ p_{3j} = r_{3j} + d \cdot n_3 \\ g(r_{1j}, r_{2j}, r_{3j}) \le 0 \end{cases} \end{aligned} \tag{39}$$

where $\boldsymbol{n} = -\boldsymbol{Ae} = (n_1, n_2, n_3)^{\mathrm{T}}$ and $\boldsymbol{e}=(1,1,1)^{\mathrm{T}}$. d is the distance parameter between the Utopia surface and the Pareto front. The larger d is, the smaller the objective function value of the feasible solution is. (r_{1j}, r_{2j}, r_{3j}) is the intersection of $\boldsymbol{n}$ and the Pareto front. $g(\cdot)$ is the model constraints.

C. MULTI-OBJECTIVE OPTIMIZATION DECISION

After obtaining a uniformly distributed Pareto front, the TOPSIS method is used to select the compromise solution. This decision method determines the positive and negative ideal points and calculates the relative closeness of the non-inferior solution. The larger the value of relative closeness is, the closer the non-inferior solution is to the positive ideal point [32]–[35]. The non-inferior solution with the largest degree of closeness is selected as the compromise solution.

The flowchart of optimization process is shown in Figure 2.

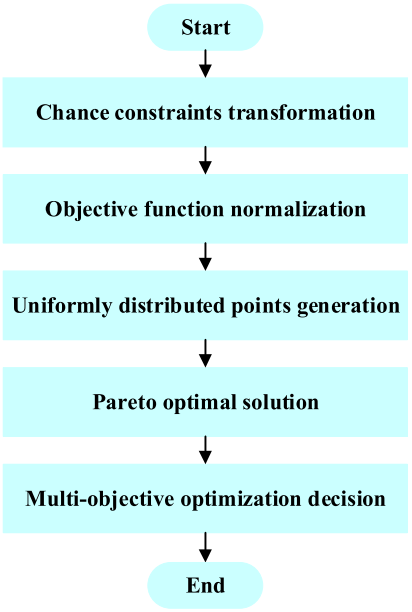

FIGURE 2. Flowchart of optimization process.

TABLE 1. Time-consuming analysis of simulation.

Parameters	IEEE 39-bus system		Guangdong Grid system
	Good atmospheric condition case	Bad atmospheric condition case	
Δt	1h		1h
Time-consuming of $G(\cdot)$	0.0449s		0.3721s
Simulation time-consuming	64.7658s	68.1827s	158.4517s

V. CASE STUDIES AND PRACTICAL DATA VALIDATION

The simulation in this article is performed on a DELL desktop computer. The computer is configured with Intel (R) Core (TM) i7-7700 CPU @ 3.60 GHz, RAM: 8.00 GB. Table 1 shows the time-consuming of the TSD model and the simulation time of each case.

The following four strategies are employed for comparison.

Strategy 1: Economic dispatch strategy without wind farms and pumped storage power plants, as

$$\min\ F = (F_C, E_C) \tag{40}$$

Strategy 2: Economic dispatch strategy for wind-thermal-storage generation system, as

$$\min\ F = (F_C, E_C) \tag{41}$$

Strategy 3: EED strategy for wind-thermal-storage generation system that considers the impact of pollutants and aims to minimize pollutants emissions, as

$$\min\ F = (F_C, E_C, E_{SO_2}) \tag{42}$$

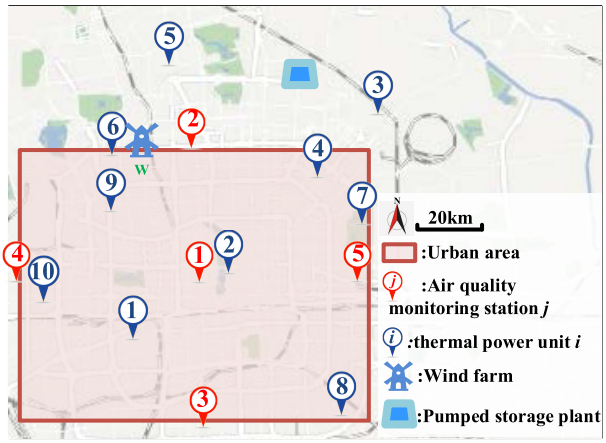

FIGURE 3. Geography of the IEEE 39-bus system case.

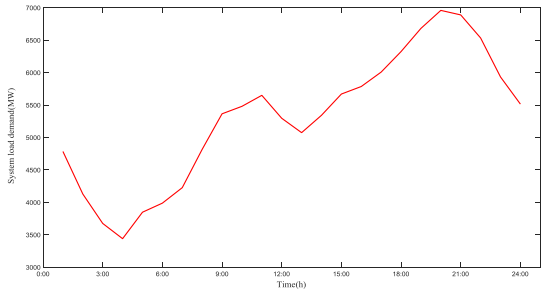

FIGURE 4. Load curves in the IEEE 39-bus system case.

Strategy 4: EED strategy for wind-thermal-storage generation system that considers the impact of pollutants and aims to minimize CPEV, as

$$\min \ F = (F_C, E_C, \overline{CPEV}) \tag{43}$$

A. IEEE 39-BUS SYSTEM CASE

Parameters of the thermal units, the wind farm and the pumped storage power plants are presented in Table 4 [36], Table 5, and Table 6 in Appendix, respectively. Figure3 and Figure4 are the geography and load curves of the IEEE 39-bus system, respectively. Two cases under opposite atmospheric conditions are studied, while T_{res} is set to be 24 h.

1) BAD ATMOSPHERIC CONDITION CASE

In this case, the wind is light or calm so that pollutants are easy to accumulate. GLPC before the scheduling day is set to zero to study the solely effects of one day's EED decision. The following points can be drawn from the simulation results in Figure 5:

a) The GLPC is significantly affected by wind speed. There is a decline in the GLPC at 5:00-7:00 in the morning and 21:00-22:00 at night. The reason is that wind speed in these two time periods increases by about 30% compared with the time before and after it. Even if the emissions are close, the GLPC will still present significant differences.

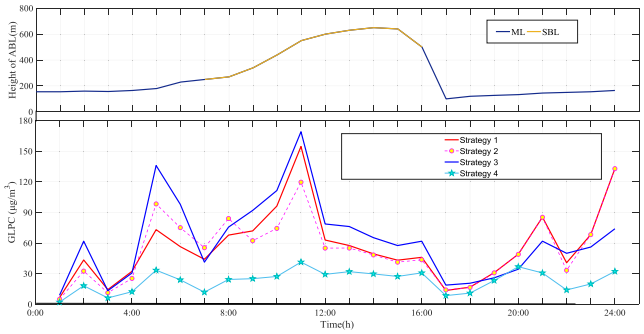

FIGURE 5. Atmospheric boundary layer height and ground-level SO_2 concentration under the four strategies in the bad atmospheric condition case.

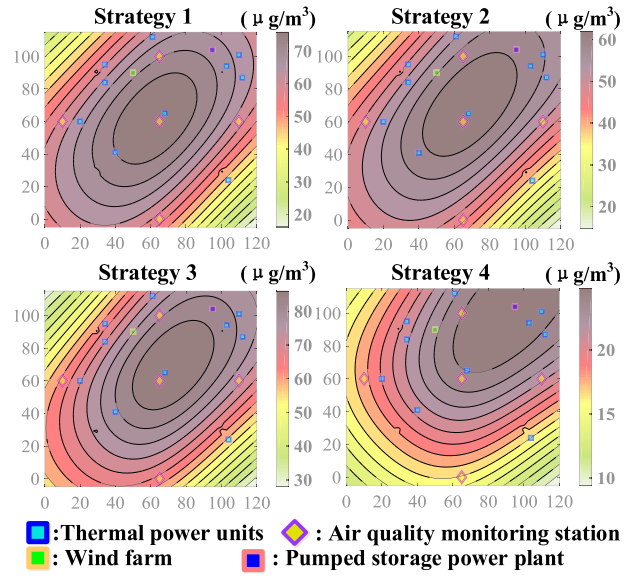

FIGURE 6. Ground-level SO_2 concentration under the four strategies at 11:00 in the bad atmospheric condition case.

b) GLPC is significantly affected by the diurnal variation of the ABL. In the early morning, GLPC increases significantly when the height of the ABL is low, and the upward dispersion of the pollutants is inhibited by the EL. By contrast, dominated by the active turbulent in ML, the pollutants quickly disperse downwards in the type of fumigation, so the GLPC rises rapidly. Especially after around 11:00 when $z_i(\tau) \geq z_{si}$, and the pollutants are directly emitted into the unstable ML, which is not easy to accumulate, so the GLPC begin to decline. After 18:00, the GLPC increases gradually since the pollutants entering the inactive SBL accumulate, which results in serious pollution.

Figure 5 and Table 2 shows that pollutant emissions decreased by 15.3% while the GLPC increases by 28.3% under Strategy 3. Comparing Strategy 4 with Strategy 1, SO_2 emissions increased by 19.2% while. the average GLPC decreases by 59.3%. It proves that the spatial and temporal distribution of pollutants should be considered in EED and the GLPC index is effective in evaluating the pollution level.

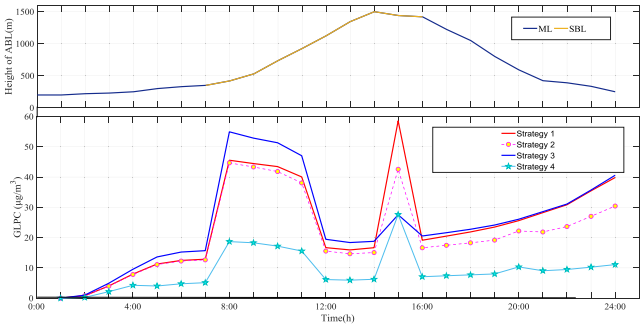

FIGURE 7. Atmospheric boundary layer height and ground-level SO_2 concentration under the four strategies in the good atmospheric condition case.

TABLE 2. Cost and emission results under four strategies.

Case	Strat-egy	Costs/ 10^4\$	CO_2 Emissions /t	SO_2 Emissions/t	SO_2 GLPC/ ($\mu g \cdot m^{-3}$)
Bad	1	314.66	3965.9	598.01	19.8435
air	2	303.87	3677.2	573.33	20.5863
quality	3	347.45	3898.3	506.75	25.4562
case	4	347.96	4835.5	712.95	8.0811
Good	1	314.66	3965.9	598.01	6.7852
air	2	286.44	3240.5	534.62	6.6905
quality	3	307.95	3165.6	450.37	7.3718
case	4	303.77	3445.6	572.13	3.0491

TABLE 3. Cost and emission results under four strategies in simulation of Guangdong grid case.

Strategy	Costs/ 10^4\$	CO_2 Emission/10^4t	SO_2 Emission/t	SO_2 GLPC/ ($\mu g \cdot m^{-3}$)
1	23163	905.68	1059.0	2.1517
2	23068	901.95	1056.0	2.1455
3	23104	901.47	1046.6	2.1199
4	23100	904.11	1065.5	1.8633

We further study the pollutants concentration distribution at 11:00 when the peak concentration occurs. The following points can be drawn from Figure 6 and Appendix A Figure 9:

a) Densely populated areas are given priority with the help of considering air pollutant diffusion. Compared with the other three strategies, the GLPC under Strategy 4 is greatly reduced. From the perspective of geographical distribution, the pollutants are mainly concentrated in the northeast of the main urban area. Under the other strategies, the pollutants are concentrated in the main urban area with high concentration levels.

b) Different pollution characteristics of units are distinguished while a target-oriented control is realized. Compared with Strategy 3, the output of Unit 2 and Unit 4 under Strategy 4 significantly decreases. The reason is that the dominant wind direction is northeast, and Unit 2 and Unit 4 are located in the upwind direction of the urban area. Meanwhile, the output of Unit 10 located in the downwind direction of the urban area increases under Strategy 4 since the emitted pollutants from it will not disperse to the urban

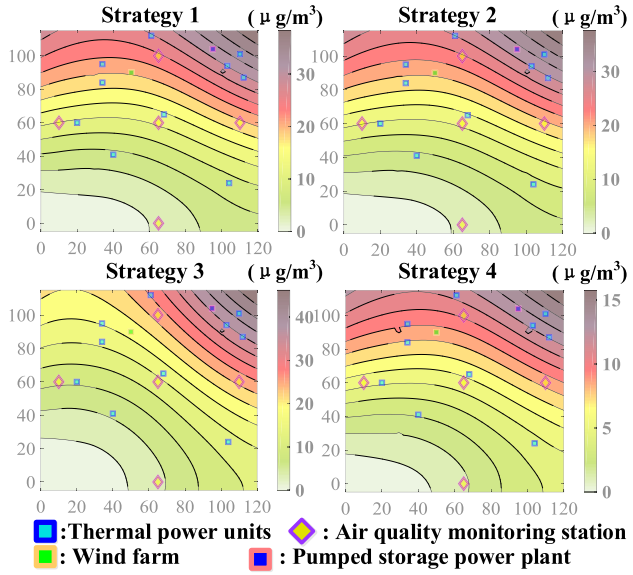

FIGURE 8. Ground-level SO_2 concentration under the four strategies at 11:00 in the good atmospheric condition case.

area. Compared with strategy 3, the output of Unit 1 also significantly decreases. The reason is that Unit 1 is located in the urban area and pollutants are easy to accumulate when the wind speed is too small. Meanwhile, the output of Unit 3 and Unit 5 increases significantly. It can be notice that Unit 3 and Unit 5 are far away from the main urban area, so their impact on the concentration of pollutants in the urban area is limited. These findings demonstrate that the proposed model can identify the thermal power plants that have a large impact on GLPC and therefore EED can be conducted in a target-oriented manner.

By contrast, Strategy 3 only considers emission amount, which prioritizes the units with small emission coefficients. The ignorance of unit location and air pollutant dispersion drives the EED decisions away from optimal solutions.

As for the pumped storage operations, we can see in Figure 11 that

a) The pumped storage power plants pump during 2:00 AM to 7:00 AM, while generates power generation is performed from 19:00 to 22:00 in the evening. It coincides with the valleys and peaks of the load. The operation of the pumped storage power plant shows obvious characteristics of diurnal variation with the diurnal variation of the system load, thus cooperating with the thermal power generation dispatching plan and achieving the reduction of pollutant emissions.

b) By contrast, the operation of pumped storage power plants under Strategy 4 coincides with not only system load but also the diurnal variation of the ABL. In the early morning when the ABL is so low that the pollutants are inhabited from dispersing downward, pumped storage is performed. During the formation and height increase of the unstable ML in the early morning, the pollutants that accumulated in SBL disperse downward rapidly under the domination of turbulent exchange in the ML, causing a sharp rise in GLPC. Pollutants disperse in type of fumigation from 9:00 to

TABLE 4. Data of thermal power plants and units in modified IEEE 39-bus system.

Units parameters	1	2	3	4	5	6	7	8	9	10
Zs /m	510	450	556	441	630	465	628	443	452	635
$P_i^{\max}$ /MW	725	1100	687	1040	646	580	508	652	564	865
$P_i^{\min}$/MW	145	220	137.4	208	129.2	116	101.6	130.4	112.8	173
DR_i/UR_i/(MW/h)	363	550	344	520	323	290	254	326	282	433
a_i /($/h)	700	660	450	680	970	370	670	665	1000	480
b_i /($/(MW/h))	16.6	25.92	19.7	16.5	17.26	22.26	27.79	27.27	16.19	27.74
c_i /($/(MW^2/h))	0.002	0.00413	0.0398	0.00211	0.00031	0.00712	0.00173	0.00222	0.00048	0.00079
d_i /(kg/h)	130	132	137.7	125	157	130	110	135	137.7	160
e_i /(kg/(MW/h))	-2.35	-2.72	-2.94	-2.36	-1.29	-2.86	-2.28	-2.36	-2.14	-1.14
g_i /(kg/(MW^2/h))	0.058	0.02	0.044	0.065	0.082	0.022	0.08	0.075	0.084	0.09
h_i/(kg/h)	111.87	195.34	155.15	152.26	134.15	198.33	101.43	152.26	126.62	142.26
l_i /(kg/(MW/h))	2.62	2.09	2.14	2.25	5.38	2.06	3.45	2.11	5.18	5.4
m_i /(kg/(MW^2/h))	0.0022	0.00018	0.0022	0.002	0.0054	0.00019	0.0025	0.0021	0.0042	0.005

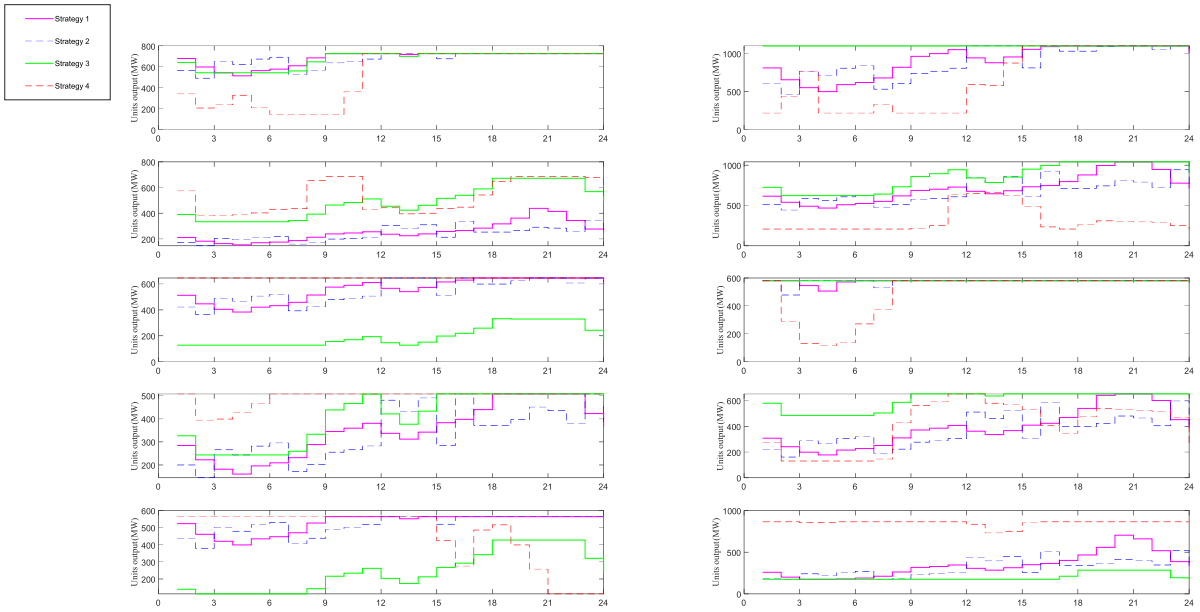

FIGURE 9. Generation schedules in the bad atmospheric condition case.

10:00 in the morning, and the concentration of pollutants rises sharply. During this period, the power generated by the pumped storage power plant can significantly alleviate the increase in GLPC. At noon, the pollutants dispersion follows the enclosed type, and the condition for the pollutants' dispersion improves. At this time, the pumped storage power plant performs pumped storage. When the load peaks at night, centralized power generation is carried out again.

2) GOOD ATMOSPHERIC CONDITION CASE

In the good atmospheric condition case, the wind speed is large, so the GLPC is relatively low.

From Figure 7, Figure8 and Table 2, the following points can be drawn:

a) Comparing the results under Strategy 2 and Strategy 3, we can see that the pollutant emission control sacrifices the generation cost but not actually reduce the average GLPC. This indicates that considering the EED problem from the perspective of pollutants emissions may increase the threat of pollutants emitted by thermal power plants to human society.

b) Comparing the results under Strategy 3 and Strategy 4 in good atmospheric condition case, we can see that the emissions are 27.0% more under Strategy 4, but the SO_2GLPC is 58.6% less. It further justifies the proposed method.

c) Comparing Strategy 1, 2, and 4, we can see that under the weather conditions where clean energy power generation plays a positive role, the method proposed in this paper can further optimize air quality.

B. GUANGDONG GRID SYSTEM CASE

Guangdong Grid system includes 59 thermal power plants, 134 thermal power units and 31 gas turbines, with a total installed capacity of 61,838 MW. The installed capacity of the wind farm is 3 245 MW while the installed capacity of pumped storage power plants is 7,300MW. The real weather data from January 5, 2017 and January 6, 2017 is used in this case [37].

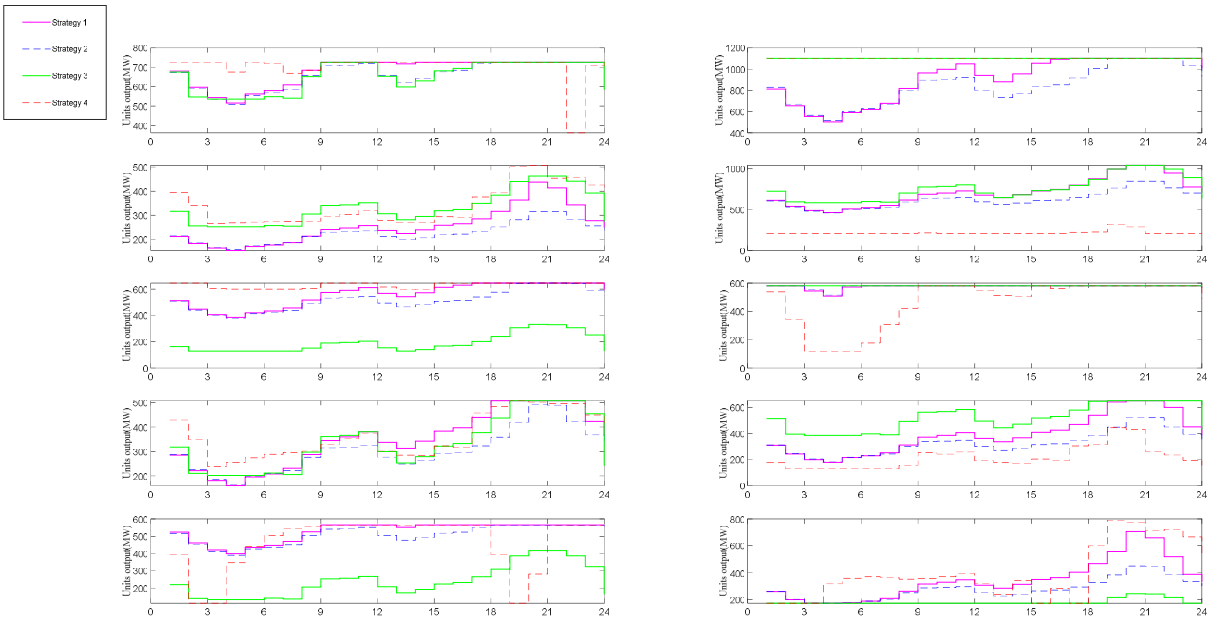

FIGURE 10. Generation schedules in the good atmospheric condition case.

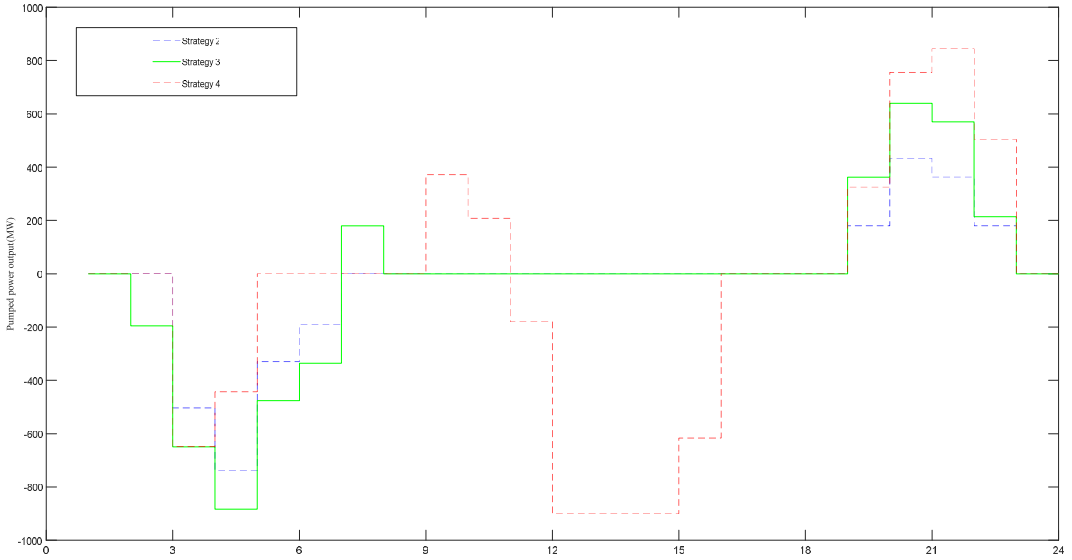

FIGURE 11. Pumped storage power plant output in the bad atmospheric condition case.

TABLE 5. Parameters of the wind farm.

v_{in}/(m/s)	v_r/(m/s)	v_{out}/(m/s)	P_r/MW	w_u/%	w_d/%
3.5	11.5	23	1000	20	50

As shown in Table 3, comparing Strategy 2 and Strategy 1, in the power system with multiple forms of energy generation, the economic cost is USD 950,000 less, carbon emissions is 37,300 tons less, and the GLPC is 0.29% less. Note that under Strategy 3, SO_2 emissions are limited to 1046.6 tons, which is actually less than that under Strategy2. By contrast, GLPC is only 1.19% less compared with Strategy 2 under Strategy 4, while a decrease of 13.15% lower SO_2 ground concentration can be realized, which further demonstrates the effectiveness of the proposed model.

VI. CONCLUSION

In this paper, we propose a multi-objective optimization dispatching model for wind-thermal-storage generation system incorporating temporal and spatial distribution control of air pollutant dispersion. Geographic grid point interpolation method is adopted in this model to evaluate the wind speed at each geographic location and along the puff center moving path. The simulation results of the IEEE 39-bus system under two atmospheric conditions show that the dispersion of pollutants indeed exhibits extremely strong spatiotemporal correlation and diurnal variation characteristics. In the time dimension, the model can coordinate multiple generation sources in the face of atmospheric condition variation. In the space dimension, the correlations between power plants location, pollutant diffusion paths and atmospheric boundary

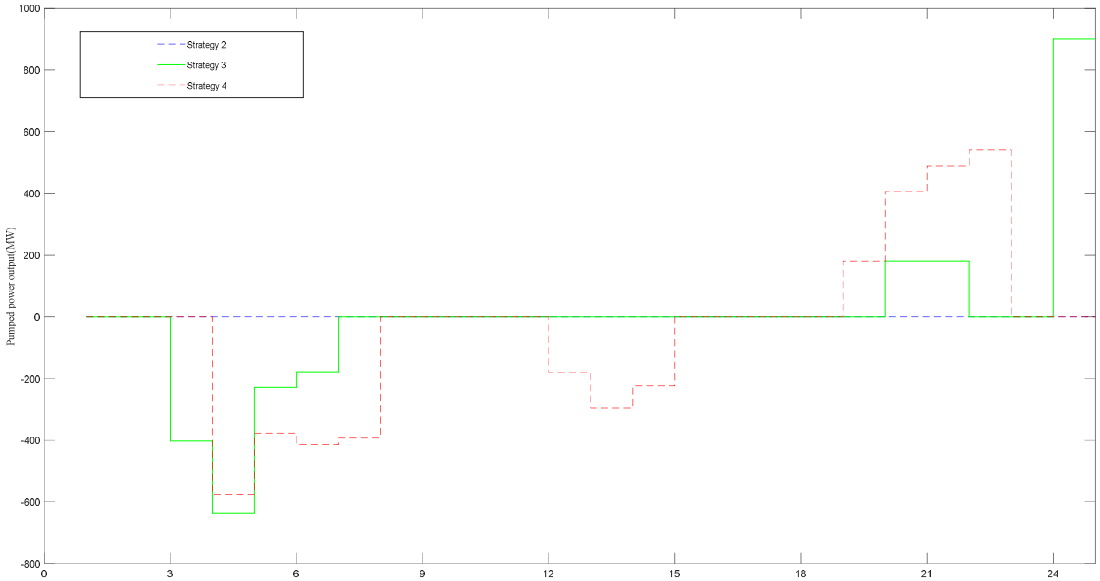

FIGURE 12. Pumped storage power plant output in the good atmospheric condition case.

TABLE 6. Parameters of the pumped storage power plant.

$P^{g}_{Ht,\min}$ /MW	$P^{g}_{Ht,\max}$ /MW	$P^{p}_{Ht,\min}$ /MW	$P^{p}_{Ht,\max}$ /MW	$E_{\mathrm{H,min}}$/MWh	$E_{\mathrm{H,max}}$/MWh	η^{g}/%	η^{p}/%
180	900	180	900	1000	7500	81	81

layers are considered. Meanwhile, the model plays an active role in improving air quality under two different atmospheric conditions, especially in the bad atmospheric condition where the pollutants are easy to accumulate and the clean energy output is limited. In this case, the GLPC is 59.3 % better under the proposed model. In Guangdong Grid system case, the result shows that the EED model plays a very active role in reducing the GLPC, and the average GLPC of SO_2 can drop by 13.15% in Guangdong province, without introducing other facilities construction and special treatment costs.

In this paper, the influence of meteorological factors, such as, rain and air humidity, and the constraints of topographical conditions have not been fully considered. The further work will focus on these factors.

APPENDIX

See Tables 4–6 and Figures 9–12.

REFERENCES

[1] World Health Organization. (2005). *WHO Air Quality Guidelines-Global Update*. Accessed: Feb. 1, 2019. [Online]. Available: http://www.euro.who.int/en/health-topics/environment-and-health/Housing-and-health/publications/pre-2009/air-quality-guidelines.-global-update-2005.-particulate-matter,-ozone,-nitrogen-dioxide-and-sulfur-dioxide

[2] G. Zhaowei, C. Qixin, and X. Qing, "Dispatching and operation of power system towards environmental synergy: Connotations and prospects," *Autom. Electr. Power Syst.*, vol. 41, no. 22, pp. 1–9, 2017.

[3] M. Miao, L. Yong, and C. Yijia, "Optimization strategy of muti-energy hybrid AC/DC power system considering environmental factors," *Autom. Electr. Power Syst.*, vol. 42, no. 4, pp. 128–134, 2018.

[4] C. Gonggui and C. Jinfu, "Environmental/economic dynamic dispatch modeling and method for power systems integrating wind farms," *Proc. CSEE.*, vol. 33, no. 10, pp. 27–35, 2013.

[5] M. J. Leppitsch and B. F. Hobbs, "The effect of NO_x regulations on emissions dispatch: A probabilistic production costing analysis," *IEEE Trans. Power Syst.*, vol. 11, no. 4, pp. 1711–1717, 1996.

[6] K. K. Mandal, S. Mandal, B. Bhattacharya, and N. Chakraborty, "Non-convex emission constrained economic dispatch using a new self-adaptive particle swarm optimization technique," *Appl. Soft Comput.*, vol. 28, pp. 188–195, 2013.

[7] C. Qixin, K. Chongqing, and X. Qing, "Mechanism and modelling approach to low-carbon power dispatch," *Autom. Electr. Power Syst.*, vol. 34, no. 12, pp. 18–23, 2010.

[8] S. J. Wang, S. M. Shahidehpour, D. S. Kirschen, S. Mokhtari, and G. D. Irisarri, "Short-term generation scheduling with transmission and environmental constraints using an augmented lagrangian relaxation," *IEEE Trans. Power Syst.*, vol. 10, no. 3, pp. 1294–1301, 1995.

[9] M. Gent and J. Lamont, "Minimum-emission dispatch," *IEEE Trans. Power App. Syst.*, vol. PAS-90, no. 6, pp. 2650–2660, Nov. 1971.

[10] Y. Li, J. Wang, D. Zhao, G. Li, and C. Chen, "A two-stage approach for combined heat and power economic emission dispatch: Combining multi-objective optimization with integrated decision making," *Energy*, vol. 162, pp. 237–254, Nov. 2018.

[11] P. Schweizer, "Determining optimal fuel mix for environmental dispatch," *IEEE Trans. Autom. Control*, vol. 19, no. 5, pp. 534–537, Oct. 1974.

[12] S. Lei, Y. Hou, X. Wang, and K. Liu, "Unit commitment incorporating spatial distribution control of air pollutant dispersion," *IEEE Trans Ind. Informat.*, vol. 13, no. 3, pp. 995–1005, Jun. 2017.

[13] K.-C. Chu, M. Jamshidi, and R. Levitan, "An approach to on-line power dispatch with ambient air pollution constraints," *IEEE Trans. Autom. Control*, vol. 22, no. 3, pp. 385–396, Jun. 1977.

[14] Y. Nan and Y. Jilai, "Generator maintenance scheduling and electric energy decomposition method considering influence of thermal power on air quality," *Autom. Electr. Power Syst.*, vol. 41, no. 6, pp. 72–79, 2017.

[15] Y. Chen, T. Yu, B. Yang, X. S. Zhang, and K. Qu, "Many-objective optimal power dispatch strategy incorporating temporal and spatial distribution control of multiple air pollutants," *IEEE Trans Ind. Informat.*, vol. 15, no. 9, pp. 5309–5319, Sep. 2019.

[16] B. Yang, T. Yu, H. Shu, J. Dong, and L. Jiang, "Robust sliding-mode control of wind energy conversion systems for optimal power extraction via nonlinear perturbation observers," *Appl. Energy*, vol. 210, pp. 711–723, Jan. 2018.

[17] B. Yang, X. Zhang, T. Yu, H. Shu, and Z. Fang, "Grouped grey wolf optimizer for maximum power point tracking of doubly-fed induction generator based wind turbine," *Energy Convers. Manage.*, vol. 133, pp. 427–443, Feb. 2017.

[18] B. Yang, L. Jiang, L. Wang, W. Yao, and Q. H. Wu, "Nonlinear maximum power point tracking control and modal analysis of DFIG based wind turbine," *Int. J. Electr. Power Energy Syst.*, vol. 74, pp. 429–436, Jan. 2016.

[19] B. Yang, T. Yu, H. Shu, Y. Zhang, J. Chen, Y. Sang, and L. Jiang, "Passivity-based sliding-mode control design for optimal power extraction of a PMSG based variable speed wind turbine," *Renew. Energy*, vol. 119, pp. 577–589, Apr. 2018.

[20] B. Yang, L. Zhong, X. Zhang, H. Shu, T. Yu, H. Li, L. Jiang, and L. Sun, "Novel bio-inspired memetic salp swarm algorithm and application to MPPT for PV systems considering partial shading condition," *J. Cleaner Prod.*, vol. 215, pp. 1203–1222, Apr. 2019.

[21] B. Yang, T. Yu, X. Zhang, H. Li, H. Shu, Y. Sang, and L. Jiang, "Dynamic leader based collective intelligence for maximum power point tracking of PV systems affected by partial shading condition," *Energy Convers. Manage.*, vol. 179, pp. 286–303, Jan. 2019.

[22] J. Weimei, *Air Pollution Meteorology*. Beijing, China: China Meteorological Press, 2004.

[23] S. Peixuan, *Atmospheric Physics*. Beijing, China: Peking Univ. Press, 2013.

[24] *Technical Methods for Making Local Emission Standards of Air Pollutants*, Standard GB/T 3840-91, Ministry of Energy and Environment of China, Standard Press of China, Beijing, China, 1992.

[25] L. Baoding, Z. Ruiqing, and W. Gang, *Uncertain Programming With Applications*. Beijing, China: Tsinghua Univ. Press, 2003, pp. 79–88.

[26] Y. Hu, Y. Li, M. Xu, L. Zhou, and M. Cui, "A chance-constrained economic dispatch model in wind-thermal-energy storage system," *Energies*, vol. 10, no. 3, p. 326, Mar. 2017.

[27] I. Das and J. E. Dennis, "Normal-boundary intersection: A new method for generating the Pareto surface in nonlinear multicriteria optimization problems," *SIAM J. Optim.*, vol. 8, no. 3, pp. 631–657, Aug. 1998.

[28] C. Roman and W. Rosehart, "Evenly distributed Pareto points in multi-objective optimal power flow," *IEEE Trans. Power Syst.*, vol. 21, no. 2, pp. 1011–1012, May 2006.

[29] Y. Liuqing, L. Shunjiang, and L. Mingbo, "Multi-objective dynamic optimal dispatch for largescale power systems considering wind power penetration," *Trans. China Electrotech. Soc.*, vol. 29, no. 10, pp. 286–295, 2014.

[30] K. Qu, S. Shi, T. Yu, and W. Wang, "A convex decentralized optimization for environmental-economic power and gas system considering diversified emission control," *Appl. Energy*, vol. 240, pp. 630–645, Apr. 2019.

[31] K. Qu, T. Yu, X. Zhang, and H. Li, "Homogenized adjacent points method: A novel Pareto optimizer for linearized multi-objective optimal energy flow of integrated electricity and gas system," *Appl. Energy*, vols. 233–234, pp. 338–351, Jan. 2019.

[32] K. Qu, T. Yu, L. Huang, B. Yang, and X. Zhang, "Decentralized optimal multi-energy flow of large-scale integrated energy systems in a carbon trading market," *Energy*, vol. 149, pp. 779–791, Apr. 2018.

[33] B. Wen, Z. Bai, and F. Wen, "Environmental/economic dispatch considering emission benefit factor in the emission trading environment," *Int. J. Energy Sector Manage.*, vol. 5, no. 3, pp. 407–415, Sep. 2011.

[34] X. S. Zhang, Z. Xu, T. Yu, B. Yang, and H. Wang, "Optimal mileage based AGC dispatch of a GenCo," *IEEE Trans. Power Syst.*, to be published, doi: 10.1109/TPWRS.2020.2966509.

[35] X. Zhang, T. Yu, B. Yang, and L. Cheng, "Accelerating bio-inspired optimizer with transfer reinforcement learning for reactive power optimization," *Knowl.-Based Syst.*, vol. 116, pp. 26–38, Jan. 2017.

[36] Z. Xiaohua, Z. Jinquan, and C. Xinying, "Multi objective commitment fuzzy modeling and optimization for energy-saving and emission reduction," *Proc. CSEE*, vol. 30, no. 22, pp. 71–76, 2010.

[37] Z. Wenbo, L. Nan, and H. Zhijiong, "Emission characteristics of thermal power in Guangdong province and influence on atmospheric environment," *Res. Environ. Sci.*, vol. 29, no. 6, pp. 810–818, 2016.

ZHUOHUAN LI received the B.S. degree in electrical engineering from the South China University of Technology, Guangzhou, China, in 2018, where he is currently pursuing the M.S. degree in electrical engineering with the School of Electric Power Engineering. His research interest includes optimal operation of power systems.

TAO YU (Member, IEEE) received the B.Eng. degree in electrical power system from Zhejiang University, Hangzhou, China, in 1996, the M.Eng. degree in hydroelectric engineering from Yunnan Polytechnic University, Kunming, China, in 1999, and the Ph.D. degree in electrical engineering from Tsinghua University, Beijing, China, in 2003. He is currently a Professor with the School of Electric Power Engineering, South China University of Technology, Guangzhou, China. His special fields of interest include nonlinear and coordinated control theory, artificial intelligence techniques in planning, and operation of power systems.

YIXUAN CHEN received the B.S. and M.S. degrees in electrical engineering from the South China University of Technology, Guangzhou, China, in 2016 and 2019, respectively. Her research interest includes the heuristic optimization techniques for low-carbon dispatch of power systems.

HANXIN ZHU received the B.S. degree in electrical engineering from the South China University of Technology, Guangzhou, China, in 2018, where he is currently pursuing the M.S. degree in electrical engineering with the School of Electric Power Engineering. His research interest includes optimal operation of power systems.

WEICONG WU received the B.S. degree in electrical engineering from Huaqiao University, Xiamen, China, in 2018. He is currently pursuing the M.S. degree in electrical engineering with the School of Electric Power Engineering. His research interest includes optimal operation of power systems.